Arabian Journal of Chemistry (2015) 8, 222–227

King Saud University

Arabian Journal of Chemistry

www.ksu.edu.sa
www.sciencedirect.com

ORIGINAL ARTICLE

# Synthesis and investigation of the physico-chemical properties of catalysts based on mixed oxides $Ce_xZr_{1-x}O_2$

S. Nousir [a], R. Maache [a], S. Azalim [a,b], M. Agnaou [b], R. Brahmi [a,*], M. Bensitel [a,*]

[a] *Laboratory of Catalysis and Corrosion of Materials, University Chouaib Doukkali, Faculty of Science El Jadida, BP. 20, El Jadida 24000, Morocco*
[b] *Laboratory of Coordination Chemistry and Analysis, University Chouaib Doukkali, Faculty of Sciences El Jadida, BP. 20, El Jadida 24000, Morocco*

Received 23 May 2011; accepted 22 July 2011
Available online 30 July 2011

**KEYWORDS**

Ethyl acetate;
VOC;
Catalysts;
Ceria;
Zirconia;
Zr–Ce oxide

**Abstract** A series of mixed oxide catalysts $Ce_xZr_{1-x}O_2$ with different compositions ($x$ = 0.93, 0.80, 0.75, 0.60, 0.55, and 0.50) were synthesized by co-precipitation technique using ammonia as the precipitant agent. Textural and structural properties of calcined ceria–zirconia oxides were characterized by nitrogen adsorption, X-ray diffraction and Raman spectroscopy. The redox properties were investigated by temperature-programmed reduction measurement using $H_2$. The procedure of preparation as well as the composition has a great influence on the structural and textural properties of mixed oxides. Fluorite type oxides were shown to be a very interesting support for the total oxidation, since these materials led to the complete decomposition of ethyl acetate at rather low temperatures. Of the synthesized materials, $Ce_{0.5}Zr_{0.5}O_2$ showed the best catalytic activity.


## 1. Introduction

Volatile organic compounds (or VOCs) are major air pollutants and treatment by catalytic oxidation is one of the most promising ways to reduce these pollutants in the atmosphere because this technique allows us to operate at low temperatures. The catalysts used for the oxidation of VOCs are classified in two groups: the noble metals like Pt, Pd, or Rd supported on a high surface area washcoat like alumina and transition metal oxides. Among these oxides we can find for example manganese oxide (Paulis et al., 2000), and ceria based materials (Kantzer et al., 2002). The development of noble metal catalysts (Pt, Pd, Rd) and transition metal oxides for

* Corresponding authors. Tel.: +212 523343003; fax: +212 523342187.
E-mail addresses: rachid.brahmi@univ-poitiers.fr (R. Brahmi), mbensitel@yahoo.fr (M. Bensitel).
Peer review under responsibility of King Saud University.

Production and hosting by Elsevier

http://dx.doi.org/10.1016/j.arabjc.2011.07.023
1878-5352 

catalytic oxidation of VOCs has been widely reported in the literature (Nousir et al., 2008; Barbier et al., 2005; Everaert and Baeyens, 2004; Van den Brink et al., 1998; Papaefthimiou et al., 1997). The catalytic system Zr–Ce–O was the subject of a number of studies (Picasso et al., 2007; Chen et al., 2001) due to the redox behavior and high oxygen storage capacity (OSC) of cerium oxide (Descorme et al., 2000; Fally et al., 2000; Trovarelli et al., 1999).

Recently, ceria-based catalysts specifically $CeO_2$-containing mixed oxides having the fluorite structure has attracted much interest, not only because of their use for the removal of post-combustion pollutants and for high strength organics from waste-water (catalytic wet oxidation) (Barbier et al., 2002; Kaspar et al., 1999), but also because of their application as catalyst for the direct oxidation of VOCs (Gutiérrez-Ortiz et al., 2004; Bozo et al., 2000).

There are multiple reasons for the use of cerium oxide in this application. It was known to stabilize the well-dispersed noble metal; to promote the water–gas shift and hydrocarbon-reforming reactions (Pengpanich et al., 2002), to have good redox properties and a high oxygen storage capacity (Otsuka et al., 1999). This capacity is related to the ability of cerium to reversibly change oxidation states between $Ce^{4+}$ and $Ce^{3+}$ by taking or giving up oxygen.

However, pure ceria has poor thermal stability properties (Fornasiero et al., 1996), consisting of $CeO_2$ sintering at higher temperatures. As a result, a new generation of ceria-zirconia mixed oxides has been developed (Kim et al. 2007). They combine the highly refractory properties of zirconia with the oxygen storage properties of ceria (Daturi et al., 1999). They show a good thermal resistance (Cuif et al., 1996; Pijolat et al., 1995) as well as enhanced redox properties and lead to better catalytic activities at lower temperatures (Boaro et al., 2002). In fact, catalytic properties are improved by modifying the metal support interface and introducing into the structure of the cerium oxide an increasing amount of zirconium, which has the features required to amplify the phenomena of oxygen transfer and catalyst stability (Madier et al., 1999; Otsuka et al 1999).

The composition and method of preparation of $Ce_xZr_{1-x}O_2$ solid solution, have an important effect on textural and structural properties, thus on catalytic performances of the final catalyst. The discussion of the structures and properties of these materials has been reviewed before (Di Monte and Kašpar, 2005a; Di Monte and Kašpar, 2005b; Inaba and Tagawa, 1996; Trovarelli, 1996; Mogensen et al., 2000). Kašpar proposed different aspects concerning the various factors related to the structure, texture, and particle size of the $Ce_xZr_{1-x}O_2$ solid solutions, as well as the concurrent effects on the chemical properties (Di Monte and Kašpar, 2005a).

The role of Ce–Zr interactions and the transfer of oxygen on the catalytic activity justify that this study has been devoted to the influence of specific surface and the Zr content on the catalytic performance of ceria. We analyze in more detail the reduction and catalytic behavior of $Ce_xZr_{1-x}O_2$ solid solutions in the complete oxidation of ethyl acetate. In particular, we have investigated the effects of introducing Zr into $CeO_2$ lattice, focusing on the structural properties, thermal stability and catalytic activity. Powder X-ray diffraction, Raman spectroscopy, temperature-programmed reduction (TPR) and surface area measurements have been performed to pursue this aim.

## 2. Experimental

### 2.1. Catalyst preparation

In this study, the $Ce_xZr_{1-x}O_2$ supports were synthesized by co-precipitation method. The mixed oxide samples were prepared from cerium nitrate ($Ce(NO_3)_3.6H_2O$, Aldrich, 99-wt%) and zirconyl nitrate ($ZrO(NO_3)_2.2H_2O$, Aldich, 99-wt%). The starting metal salts were dissolved in distilled water with the appropriate concentration in order to have the specified Ce/Zr ratios. The ratio between the metal salts was altered depending on the desired solid solution concentration: $Ce_xZr_{1-x}O_2$ in which $x = 0.93$, 0.80, 0.75, 0.60, 0.55, and 0.50. Then, 12 ml of ammonia solution (25-wt%) was added dropwise after which the stirring was stopped. The resulting product was filtered, washed with dilute ammonia solution and distilled water, and dried at 393 K overnight, then calcined in air at 723 K for 6 h.

### 2.2. Characterization

The specific surface areas of the prepared powders were analyzed by nitrogen adsorption at 77 K using the BET method (Micrometrics ASAP 2010). Prior to the analysis, the samples were outgassed to eliminate volatile adsorbents on the surface at 453 K for one night under high vacuum.

The structures of the ceria-zirconia mixed oxide catalysts were characterized by X-ray diffraction (Siemens D5005) with $Cu_{K\alpha}$ radiation ($\lambda = 1.5406$ Å). The X-ray tube was operated at 40 kV and 30 MA. Samples were scanned from 5° to 90° for 2θ, and the X-ray diffraction line positions were determined with a step size of 0.04° and a counting time of 2 s per step. The patterns recorded were compared to the powder diffraction files – 2002 ICDD PDF database for the identification of the crystal structures. The average crystallite size, D, was calculated by using the Scherrer equation: $D = 0.9^* \lambda/\beta \cos\theta$; where $\lambda$ is the wavelength of the X-ray, $\theta$ is the diffraction angle, $\beta = (\beta_m^2 - \beta_s^2)^{1/2}$ is the corrected half-width, $\beta_m$ is the half-width of experimental reflection and $\beta_s$ is the half-width of $LaB_6$ standard sample.

FT-Raman measurement was used in order to confirm the fluorite structure of the mixed oxides with cubic symmetry. It was performed in the region 0–3500 $cm^{-1}$ using a Bruker RFS100 instrument. The laser power was ca. 400 Mw.

Reduction behavior of the catalysts was determined by temperature-programmed reduction (TPR) experiments. After the standard cleaning pre-treatment in Ar (40 $cm^3$ $min^{-1}$) at 403 K for 1 h, the reduction was carried out in a flow of $H_2$ (5%)/Ar (20 $cm^3$ $min^{-1}$) from room temperature (RT) to 1173 K at a heating rate of 10 K $min^{-1}$.

The catalytic activity of the samples was evaluated with the complete oxidation of ethyl acetate in air. During the reaction tests, carbon dioxide and water were analyzed as reaction products. Ethyl acetate conversion was calculated from $CO_2$ appearance.

$CO_2$ production was followed with an online IR detector (Sensotran IR) and water appearance by GC–TCD (HP 5890). Light-off curves were obtained by heating the catalyst (200 mg) from RT up to 673 K in a fixed bed reactor with the heating rate of 2.5 K $min^{-1}$ in a 510 ml $min^{-1}$ air stream

containing 467 ppm of ethyl acetate. GHSV used was $10^{3-1}0^5\ h^{-1}$.

## 3. Results and discussion

### 3.1. Specific surface area and isotherms

The BET surface areas, pore volumes and pore sizes of ceria-zirconia mixed oxide catalysts are summarized in Table 1. It can be seen that, in the first time, the surface areas increase until the addition of 25% of zirconium and then decreased. The maximum surface area is obtained for ceria doped with 25% of zirconium. The average pore diameters in these catalysts were 32–46 Å and the pore volumes are similar except for $Ce_{0.75}Zr_{0.25}O_2$.

Fig. 1 compares the nitrogen adsorption/desorption isotherms of $Ce_xZr_{1-x}O_2$ ($x$ = 0.93, 0.80, 0.75, 0.60, 0.55, and 0.50). All the samples exhibited isotherms of type IV associated with mesoporous solids according to the IUPAC classification (Colón et al., 1998). Their profiles of pore size distribution are shown in Fig. 2. $Ce_{0.75}Zr_{0.25}O_2$ has the higher pore volume and pore diameter than the other samples.

### 3.2. X-ray diffraction and Raman spectroscopy

It is generally accepted that the crystal structure of a $CeO_2$–$ZrO_2$ solid solution is dependent on chemical composition and on synthesis procedure. The diffraction patterns for the Ce-Zr mixed oxides calcined at 1073 K in the whole compositional range are compared in Fig. 3 All graphics showed well-defined peaks corresponding to a fluorite structure similar to those observed in the literature for $CeO_2$ (PDF No. 43-1002).

No evidence for extra peaks corresponding to $ZrO_2$ was observed in any XRD patterns of $Ce_xZr_{1-x}O_2$. This suggests that the incorporation of $ZrO_2$ into the $CeO_2$ lattice leads to formation of solid solution while maintaining the fluorite structure where $x \leqslant 0.5$, this results will be confirmed by FT-Raman spectroscopy. However, it is shown in Fig. 3 that the diffraction peaks were shifted systematically to higher Bragg angles with increasing $ZrO_2$ content. This observation was attributed to the shrinkage of lattice due to the replacement of $Ce^{4+}$ (1.09 Å) with smaller cation radius $Zr^{4+}$ (0.86 Å).(Otsuka et al., 1999).

The unit cell parameters and the crystallite sizes are calculated using the (111) plane for $Ce_xZr_{1-x}O_2$ solid solutions using Diffract-at and U-Fit software. Each peak profile was fitted using mathematical function (diffract-at program) in order to determine the position and the full width at half maximum (FWHM) of each peak with a sufficient accuracy. The results are listed in Table 2.

**Table 1** Textural parameters of the catalysts $Ce_xZr_{1-x}O_2$ calcined at 450 °C.

| Samples | BET surface area ($m^2/g$) | Pore Volume ($cm^3/g$) | Average pore diameter (Å) |
|---|---|---|---|
| $Ce_{0.93}Zr_{0.07}O_2$ | 83 | 0.067 | 32 |
| $Ce_{0.80}Zr_{0.20}O_2$ | 107 | 0.121 | 45 |
| $Ce_{0.75}Zr_{0.25}O_2$ | 196 | 0.212 | 43 |
| $Ce_{0.70}Zr_{0.30}O_2$ | 115 | 0.097 | 34 |
| $Ce_{0.60}Zr_{0.40}O_2$ | 107 | 0.091 | 34 |
| $Ce_{0.55}Zr_{0.45}O_2$ | 102 | 0.087 | 34 |
| $Ce_{0.50}Zr_{0.50}O_2$ | 94 | 0.108 | 46 |

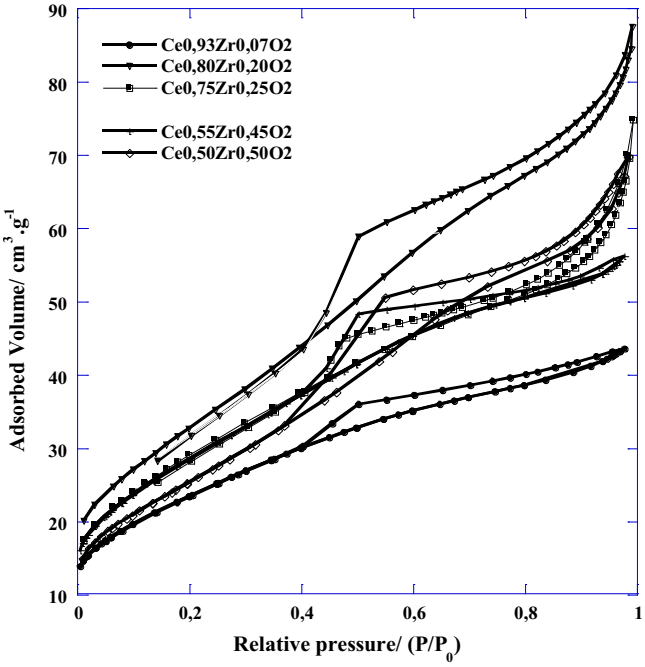


**Figure 1** N2 Adsorption/desorption isotherms on different $Ce_xZr_{1-x}O_2$ mixed oxides.

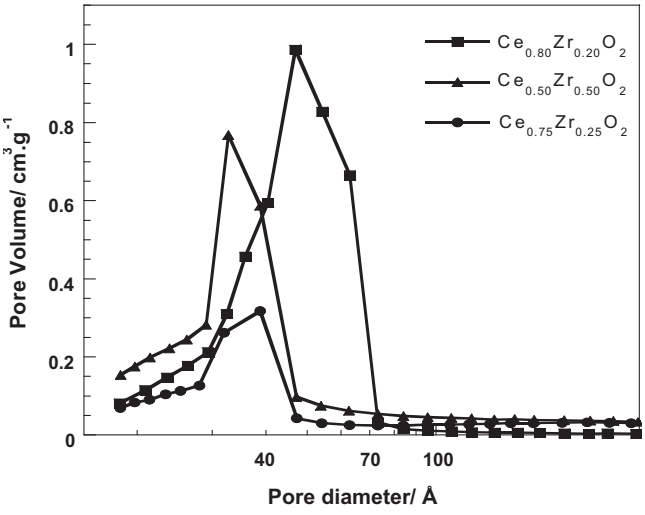


**Figure 2** Pore size distribution of $Ce_xZr_{1-x}O_2$ mesoporous mixed oxides calcined at 723 K.

The plots of the cell parameters versus the nominal composition follow a linear correlation for Zr content up to molar 50% (Fig. 4). They decrease systematically with an increase in $ZrO_2$ content. This evidences that Vegard's law is obeyed for the cubic solid solution phases and, therefore, the lattice parameter can be considered as a measure of the composition of a fluorite like solid solution phase. The crystallite size determined by the Scherrer equation was in the range of 6.9–7.6 nm for all the powders calcined at 1073 K, while those calcined at 723 K presented crystallite sizes in the range of 4.6–5.1 nm

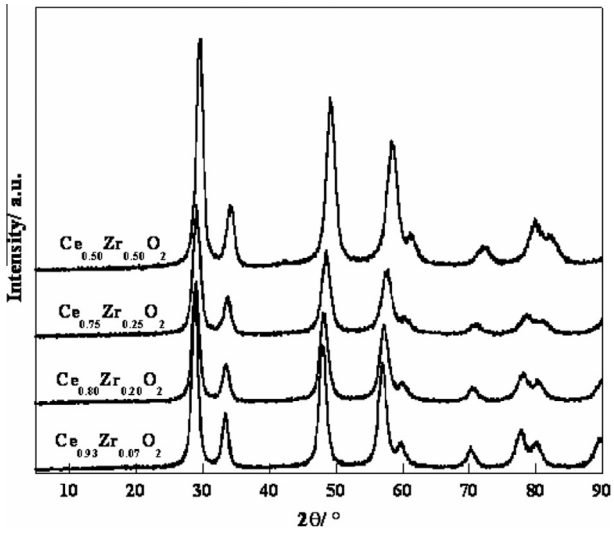


**Figure 3** XRD patterns for $Ce_xZr_{1-x}O_2$ mixed oxides catalysts calcined at 1073 K.

**Table 2** Crystallographic parameters of the $Ce_xZr_{1-x}O_2$ mixed oxides.

| Samples | T (K) | $d_{111}$ spacing (Å) | Cell parameters (Å) | Crystallite size (Å) |
|---|---|---|---|---|
| $Ce_{0,80}Zr_{0,20}O_2$ * | 723 | 3.0884 | 5.3499 | 51 |
| $Ce_{0,50}Zr_{0,50}O_2$ ** | | 3.0324 | 5.2376 | 46 |
| $Ce_{0,80}Zr_{0,20}O_2$ * | 1073 | 3.0872 | 5.3526 | 76 |
| $Ce_{0,75}Zr_{0,25}O_2$ * | | 3.0733 | 5.3267 | 71 |
| $Ce_{0,70}Zr_{0,30}O_2$ ** | | 3.0596 | 5.2964 | 69 |
| $Ce_{0,50}Zr_{0,50}O_2$ ** | | 3.0190 | 5.2263 | 69 |

* ($Ce_{0.75}Zr_{0.25}O_2$, ICDD file No. 28-0271): $a = b = c = 5.349$ Å (cubic).
** ($Ce_{0.60}Zr_{0.40}O_2$ ICDD file No. 38-1439): $a = b = c = 5.304$ Å (cubic).

(Table 2). The values of the crystal size do not change very much with increasing temperature, indicating that the sintering process is not remarkable.

In order to assign the actual phase in $Ce_xZr_{1-x}O_2$ samples with $x \leqslant 0.5$, the Raman spectra of $CeO_2$–$ZrO_2$ and $ZrO_2$ oxides calcined at 623 K were collected and the results are shown in

Fig. 5. The Raman spectra of pure ceria display only one peak at 465 $cm^{-1}$ due to the $F_{2g}$ Raman active mode of a cubic fluorite structure. This can be regarded as a symmetric O–Ce–O stretching, as expected on the basis of the factor group analysis and in consistence with the literature information (Wang et al., 2001; Kanakaraju et al., 1997; Weber et al., 1993). In the Raman spectrum of zirconia sample, no bands are detected. The Raman spectra for all

$Ce_xZr_{1-x}O_2$ samples (where $x \leqslant 0.5$), showed only one strong adsorption peak centered at about 470 $cm^{-1}$, which is typical of the $F_{2g}$ Raman active mode of a cubic fluorite structure (Fig. 5). These results are in good agreement with the XRD results, which also show only the cubic fluorite structure type. The broadening of the peak may be due to the substitution of $Zr^{4+}$ by $Ce^{4+}$ cations. In the range of 580–650 $cm^{-1}$, we observe a very weak intensity shoulder due to the presence

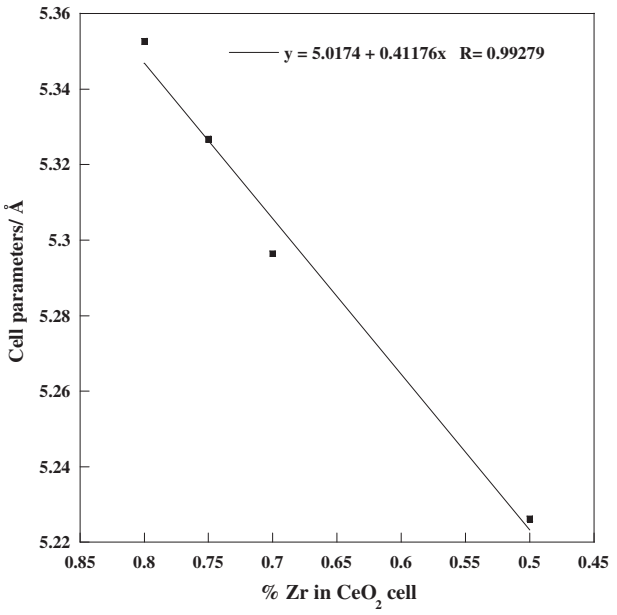


**Figure 4** Plot of the cell parameters versus the Zr content in the cubic phases calcined at 1073 K.

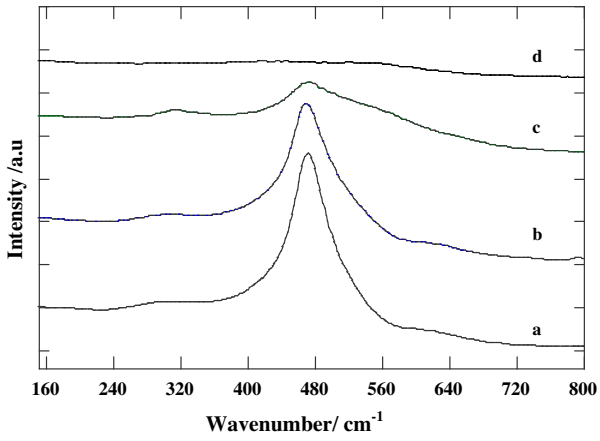


**Figure 5** Raman spectra of the Ce–Zr mixed oxides calcined at 723 K: (a) $Ce_{0.80}Zr_{0.20}O_2$, (b) $Ce_{0.75}Zr_{0.25}O_2$, (c) $Ce_{0.50}Zr_{0.50}O_2$and (d) $ZrO_2$.

of oxygen vacancies (Colón et al., 1998). The oxygen vacancies were formed by introduction of $Zr^{4+}$ into fluorite-like lattice of ceria, which generate the structural defects in the lattice of $CeO_2$ attributable to the different sizes of two ionic radii.

### 3.3. Temperature programed reduction under $H_2$

Ceria and Ce-based oxides are known for their easy reducibility. This ability is related to the capability of cerium to reversibly change oxidation states between $Ce^{4+}$ and $Ce^{3+}$. They can store oxygen when they are in contact with an oxidative atmosphere, and release oxygen when they are in the presence of a reductive atmosphere. Reducibility of the prepared materials was examined by temperature-programmed reduction (TPR) measurements using hydrogen, which can provide

insights into low- and high-temperature interaction between $H_2$ and the surface. The (TPR) profile of $CeO_2$ showed two-peak pattern, which suggest the reduction of the pure $CeO_2$–$Ce_2O_3$ taken place in two stages (Gutiérrez-Ortiz et al., 2005; Yao and Yao, 1984).

The first low temperature signal located at around 773 K is due to the reduction of the most easily reducible surface capping oxygen of ceria while removal of bulk oxygen was suggested as the cause of the high temperature signal at ca. 1173 K. These results found by Gutiérrez-Ortiz et al (2005) are similar to those reported by other authors (Yao and Yao, 1984). Comparing with the other result, TPR of ceria prepared by precipitation shows two peaks associated to surface and bulk reduction, respectively, at ca. 820 K and 1100 K (Terribile et al., 1999). but for ceria synthesized by pH-controlled nitrate–glycine gel-combustion process, the two peaks are placed at ca. 653 K and 1073 K corresponding the results of (Larrondo et al., 2005). In contrast, $ZrO_2$ is not reduced in the temperature range of 273–1173 K.

Introduction of smaller isovalent cations, such as Zr into the fcc cell of ceria, results in a defective fluorite structure with increased oxygen mobility. The TPR profiles of the mixed oxides $CeO_2$–$ZrO_2$ with $x = 0.80$, 0.75, and 0.5 are presented in Fig. 6. The reduction bands for the three compositions located at 814, 811, and 803 K, respectively, with a shoulder at ca. 643 K could be assigned to the reduction of surface and subsurface $Ce^{4+}$. Moreover, no clear kinetic distinction is observed between the redox processes occurring at the surface and in the bulk, as it is the case for ceria (Perrichon et al., 1994). This is in agreement with high mobility of the oxygen species in the solid solution. These results clearly showed that the introduction of $ZrO_2$ strongly modified the reduction behavior of $CeO_2$ by shifting main $H_2$ consumption to a lower temperature and by increasing oxygen mobility in the bulk.

### 3.4. Catalytic activities

Fig. 7 shows the light-off curves for different $Ce_xZr_{1-x}O_2$ calcined at 723 K. The total oxidation of ethyl acetate was carried out with a heating rate of 2.5 K $min^{-1}$. The total oxidation was followed by the production of $CO_2$. The activities of the catalysts are frequently characterized by two parameters, $T_{50}$ and $T_{90}$, which can be visualized with the light-off curves and are also summarized in Table 3. $T_{50}$ refers to the temperature needed to reach 50% conversion, and is widely used to compare catalytic activity, while $T_{90}$ is the temperature for 90% conversion.

The oxidation of ethyl acetate on CeZr catalysts begins around 473 K. At this temperature a small peak appears, that may be due to the adsorption of ethyl acetate on the surface of support (Paulis et al., 2000). In addition, some part of $CO_2$ that is formed during the oxidation reaction can also stay adsorbed when it is produced. The oxidation of VOCs is an exothermic reaction, which produces a local increase of temperature on the catalyst surface leading to simultaneous desorption of ethyl acetate and the products ($H_2O$ and $CO_2$). The ethyl acetate adsorbed can be oxidized, producing $CO_2$ and more heat. Therefore, the peak of $CO_2$ is the result of all processes involved in low temperature range. Cordi and Falconer (1996) have shown the adsorption of VOCs on $Al_2O_3$ prior to their oxidation on palladium, but they do not signal a coupling between the oxidation process and adsorption–desorption. In parallel, Bowker and Cassidy (1998) studied the explosive nature of adsorbed acetates on $Rh/Al_2O_3$ and they reached the same conclusion as us.

Catalytic activity was observed to be a function of Ce/Zr ratio of the solid solution. We found out that the mixed oxide,

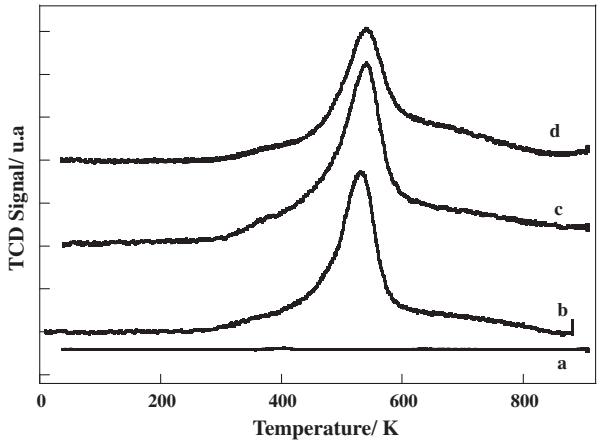


**Figure 6** H2-TPR profiles of the $Ce_xZr_{1-x}O_2$ catalysts calcined at 723 K: (a) $ZrO_2$, (b) $Ce_{0.50}Zr_{0.50}O_2$, (c) $Ce_{0.75}Zr_{0.25}O_2$ and (d) $Ce_{0.80}Zr_{0.20}O_2$.

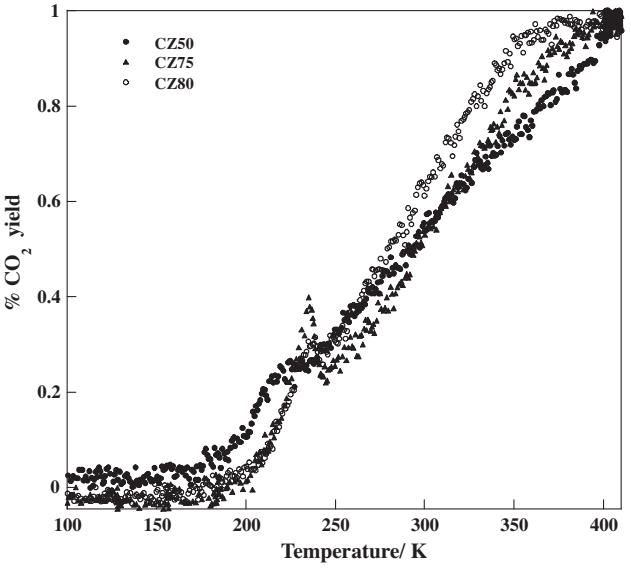


**Figure 7** Light-off curves for ethyl acetate complete oxidation over different $Ce_xZr_{1-x}O_2$ catalysts.

**Table 3** $T_{50}$ and $T_{90}$ temperatures of ethyl acetate decomposition over $Ce_xZr_{1-x}O_2$ catalysts.

| Samples | $T_{50\%}$ (k) | $T_{90\%}$ (k) |
|---|---|---|
| $Ce_{0,80}Zr_{0,20}O_2$ | 567 | 665 |
| $Ce_{0,75}Zr_{0,25}O_2$ | 568 | 639 |
| $Ce_{0,50}Zr_{0,50}O_2$ | 552 | 618 |

which presented the same molar content of both metals, i.e., $Ce_{0.50}Zr_{0.50}O_2$ has higher activity than $Ce_{0.80}Zr_{0.20}O_2$ and $Ce_{0.75}Zr_{0.25}O_2$. Even if $Ce_{0.50}Zr_{0.50}O_2$ has lower specific surface area than $Ce_{0.75}Zr_{0.25}O_2$ and $Ce_{0.80}Zr_{0.20}O_2$, it shows the highest activity. As shown in Fig. 6. $Ce_{0.50}Zr_{0.50}O_2$ is more reducible. Hence, it is clear that catalytic activity depends on the redox properties of the mixed oxides. In addition, the catalytic activity is related also to the structural properties of the catalysts. It has been observed with Ce–Zr that the oxygen mobility is dependent on structural features. For example, the cubic phase favors oxygen mobility in Ce–Zr–O system more than the tetragonal or monoclinic phases (Fornasiero et al., 1995).

## 4. Conclusion

The incorporation of Zr into the $CeO_2$ structure forming a solid solution can modify the redox behavior of the material without changing the structure of $Ce_xZr_{1-x}O_2$ when $x \leqslant 0.5$. The catalytic activity of $CeO_2$ in ethyl acetate oxidation was also enhanced by the incorporation of Zr into the structure. The catalytic activity is more dependent on the structure and the redox properties of the tested materials than on the specific surface area. The optimal formula with highest activity was achieved with $Ce_{0.50}Zr_{0.50}O_2$. The activity of the catalysts is high enough to start the oxidation at lower temperatures, close to those at which the adsorption and desorption of different species have taken place.

## References


Barbier Jr., J., Oliviero, L., Renard, B., Duprez, D., 2005. Top. Catal. 33, 77.

Barbier Jr., J., Oliviero, L., Renard, B., Duprez, D., 2002. Catal. Today 75, 29.

Boaro, M., Trovarelli, A., Hwang, J.H., Mason, T.O., 2002. Solid States Ionics 147, 85.

Bozo, C., Guilhaume, N., Garbowski, E., Primet, M., 2000. Catal. Today 59, 33.

Bowker, M., Cassidy, T.J., 1998. J. Catal. 174, 65.

Chen, H., Sayari, A., Adnot, A., Larachi, F., 2001. Appl. Catal. B. 32, 195.

Colón, G., Pijolat, M., Valdivieso, F., Vidal, H., Kaspar, J., Finocchio, E., Daturi, M., Binet, C., Lavalley, J.C., Baker, R.T., Bernal, S., 1998. J. Chem. Soc., Faraday Trans. 94, 3717.

Cuif, J., Blanchard, G., Touret, O., Marczi, M., Quémeré, E., 1996. SAE. Tech. Pap. SER., 969106

Daturi, M., Finocchio, E., Binet, C., Lavalley, J.C., Fally, F., Perrichon, V., 1999. J. Phys. Chem. B. 103, 4884.

Descorme, C., Madier, Y., Duprez, D., 2000. J. Catal. 196, 167.

Di Monte, R., Kašpar, J., 2005a. Catal. Today 100, 27.

Di Monte, R., Kašpar, J., 2005b. J. Mater. Chem. 15, 633.

Cordi, E.M., Falconer, J.L., 1996. J. Catal. 162, 104.

Everaert, K., Baeyens, J., 2004. J. Hazard. Mater. B. 109, 113.

Fally, F., Perrichon, V., Vidal, H., Kaspar, J., Blanco, G., Pintado, J.M., Bernal, S., Colon, G., Daturi, M., Lavally, J.C., 2000. Catal. Today 59, 373.

Fornasiero, P., Balducci, G., Di Monte, R., Kaspar, J., Sergo, V., Gubitosa, G., Ferrero, A., Graziani, M., 1996. J. Catal. 164, 173.

Fornasiero, P., Di Monte, R., Rao, G.R., Kaspar, J., Meriani, S., Trovarelli, A., Graziani, M., 1995. J. Catal. 151, 168.

Gutiérrez-Ortiz, J.I., de Rivas, B., López-Fonseca, R., González-Velasco, J.R., 2004. Appl. Catal. A. 269, 147.

Gutiérrez-Ortiz, J.I., de Rivas, B., López-Fonseca, R., González-Velasco, J.R., 2005. Therm. Anal. Calorim. 80, 225.

Inaba, H., Tagawa, H., 1996. Solid State Ionics 83, 1.

Kanakaraju, S., Mohan, S., Sood, A.K., 1997. Thin Solid Films 305, 191.

Kantzer, E., Döbber, D., Kiebling, D., Wendt, G., 2002. Stud. Surf. Sci. Catal. 143, 489.

Kaspar, J., Fornasiero, P., Graziani, M., 1999. Catal. Today 50, 285.

Kim, J.R., Myeong, W.J., Ihm, S.K., 2007. Appl. Catal. B. 71, 57.

Larrondo, S., Vidal, M.A., Irigoyen, B., Craievich, A.F., Lamas, D.G., Fabregas, I.O., Lascalea, G.E., Reca, N.E.W.d., Amadeo, N., 2005. Catal. Today, 53–108.

Madier, Y., Descorme, C., Le Govic, A.M., Duprez, D., 1999. J. Phys. Chem. B. 103, 10999.

Mogensen, M., Sammes, N.M., Tompsett, G.A., 2000. Solid State Ionics 129, 63.

Nousir, S., Keav, S., Barbier Jr., J., Bensitel, M., Brahmi, R., Duprez, D., 2008. Appl. Catal. B. 84, 723.

Otsuka, K., Ye, W., Nakamura, M., 1999. Appl. Catal. A. 183, 317.

Papaefthimiou, P., Ioannides, T., Verykios, X.E., 1997. Appl. Catal. B: Environ. 13, 175.

Paulis, M., Gandia, L.M., Gil, A., Sambeth, J., Odriozola, J.A., Montes, M., 2000. Appl. Catal. B. 26, 37.

Pengpanich, S., Meeyoo, V., Rirksomboon, T., Bunyakiat, K., 2002. Appl. Catal. A. 234, 221.

Perrichon, V., Laachir, A., Touret, O., Bergeret, G., Fréty, R., Tournayan, L., 1994. J. Chem. Soc., Faraday Trans. 90, 773.

Picasso, G., Gutiérrez, M., Pina, M.P., Herguido, J., 2007. J. Chem. Eng. Data 126, 119.

Pijolat, M., Prin, M., Soustelle, M., Touret, O., Nortier, P., 1995. J. Chem. Soc., Faraday Trans. 91, 3491.

Terribile, D., Trovarelli, A., de Leitenbourg, C., Primavera, A., Dolcetti, G., 1999. Catal. Today 47, 133.

Trovarelli, A., de Leitenbourg, C., Boaro, M., Dolcetti, G., 1999. Catal. Today 50, 353.

Trovarelli, A., 1996. Catal. Rev. Sci. Eng. 38, 439.

Van den Brink, R.W., Louw, R., Mulder, P., 1998. Appl. Catal. B. 16, 219.

Wang, S., Wang, W., Zuo, J., Qian, Y., 2001. Mater. Chem. Phys. 68, 246.

Weber, W.H., Hass, K.C., McBride, J.R., 1993. Phys. Rev. B. 48, 178.

Yao, H.C., Yao, Y.F.Y., 1984. J. Catal. 86, 254.